Optical Spectra and Crystal-Field Levels of [Cm(H2O)9]3+ Ions with C3h Symmetry in Isotypic Rare-Earth Triflate and Ethyl Sulfate Salts

ARTICLE *in* THE JOURNAL OF PHYSICAL CHEMISTRY C · JANUARY 2009

Impact Factor: 4.77 · DOI: 10.1021/jp808491k

4 AUTHORS, INCLUDING:

Patric Lindqvist-Reis
Karlsruhe Institute of Technology
55 PUBLICATIONS **977** CITATIONS
SEE PROFILE

N. M. Edelstein
University of California, Berkeley
367 PUBLICATIONS **7,150** CITATIONS
SEE PROFILE

Optical Spectra and Crystal-Field Levels of $[Cm(H_2O)_9]^{3+}$ Ions with C_{3h} Symmetry in Isotypic Rare-Earth Triflate and Ethyl Sulfate Salts

Patric Lindqvist-Reis,*,† Clemens Walther,† Reinhardt Klenze,† and Norman M. Edelstein‡

Institut für Nukleare Entsorgung, Forschungszentrum Karlsruhe, P.O. Box 3640, 76021, Karlsruhe, Germany, and Lawrence Berkeley National Laboratory, Berkeley, California 94720-8175

Received: September 24, 2008; Revised Manuscript Received: October 30, 2008

Fluorescence emission and excitation spectra of $[Cm(H_2O)_9]^{3+}$ ions with regular and distorted tricapped trigonal prismatic coordination geometries are reported at temperatures of 293 and 20 K. The Cm^{3+} impurities are incorporated into the hexagonal crystal lattices of the isotypic $[M(H_2O)_9](CF_3SO_3)_3$ (M = La (**1**), Y (**2**)), and $[Y(H_2O)_9](C_2H_5SO_4)_3$ (**3**) salts, and into the low symmetry $[La(H_2O)_9]Cl_3 \cdot 15\text{-crown-}5 \cdot H_2O$ (**4**) salt. Small but significant structural differences in the MO_9 polyhedra influence the crystal-field levels of the $^8S'_{7/2}$ ground-state and the $^6D'_{7/2}$ excited-state multiplets. Thus, the total $^6D'_{7/2}$ splitting is smaller in **1**−**3** (376−393 cm^{-1}) than in **4** (430 cm^{-1}), which explains the marked blue shifts of the emission spectra of **1**−**3** to those of **4** and Cm^{3+}(aq) at 293 K. The transitions between the ground state and the two lowest crystal-field levels of the $^6D'_{7/2}$ multiplets in **1**−**3** give rise to narrow fluorescence lines at the emitting level at 20 K, resolving the crystal-field levels of the ground state as sharp and narrowly spaced lines. The total ground-state splittings in **1** (8.0 cm^{-1}), **2** (6.0 cm^{-1}), and **3** (7.5 cm^{-1}) are about three to four times larger than those for Cm^{3+} in $LaCl_3$ (2.0 cm^{-1}), but four to six times smaller than those for Cm^{3+} in $[Y(H_2O)_8]Cl_3 \cdot 15\text{-crown-}5$ (35 cm^{-1}). Inhomogeneous line broadening prevents resolving the ground multiplet levels in **4**. Vibronic side bands associated with the $^8S'_{7/2}-{}^6D'_{7/2}$ transition are observed in the low temperature emission and excitation spectra. The intensities of these side bands are <1% of the parent electronic transition, the stronger ones being located below ~400 cm^{-1} and correspond to various CmO_9 skeletal modes. The luminescence lifetimes in **1**−**4** are between 63 and 74 μs.

Introduction

The structural and dynamic properties of hydrated trivalent actinide (An) ions in aqueous solution have been the subject of several recent experimental[1−6] and theoretical[7−9] studies. The Cm^{3+} ion has favorable luminescence properties such as high sensitivity and high quantum yield and is frequently used as a luminescence probe in laboratory systems at trace level concentrations by means of time-resolved laser-induced fluorescence spectroscopy (TRLFS).[10] The Cm^{3+} ion also acts as an analogue for other An^{3+} ions of similar ionic radii as the solution behavior of the trivalent actinide ions is rather similar. Cm^{3+} ($\tau_{1/2} = 3.4 \times 10^5$ years) is the isotope of choice because its long half-life reduces radiation effects to negligible amounts. However, the scarcity of this isotope (Cm^{3+} is available only in milligram quantities) restricts the number of studies of its complexes in solution as well as the preparation of solid compounds. To date, only a handful of crystal structures of curium(III) compounds are known,[11] including the newly reported $[Cm(H_2O)_9](CF_3SO_3)_3$ structures at 100 and 293 K.[1,2]

In dilute aqueous solution (pH <6; $T \sim 300$ K) the hydrated Cm^{3+} ion is most probably coordinated to nine water molecules arranged in a tricapped trigonal prism (TTP).[12] This is consistent with recent EXAFS and high-energy X-ray scattering studies on 10 and 500 mM curium(III) aqueous solutions at room temperature.[1,2] The results indicated TTP coordination geometry for the Cm^{3+} aqua ion, with six shorter and three longer Cm−O distances at a mean distance of ~2.48 Å. Hence, the local structure of Cm^{3+} in aqueous solution appears to be similar to that of Cm^{3+} in $[Cm(H_2O)_9](CF_3SO_3)_3$, which indeed features six shorter prismatic and three longer capping Cm−O distances at a mean distance of 2.48−2.49 Å.[1,2] These experimental findings are consistent with recent molecular dynamics (MD) simulations on Cm^{3+}(aq) and density functional theory (DFT) calculations on different Cm^{3+} aqua clusters.[7,8] In the MD study,[7] using ab initio calculated intermolecular potentials, the nona-hydrated aqua species with TTP geometries was shown to be more stable than octahydrated species in aqueous solution at 300 K, while with increasing temperature the amount of the latter species was found to increase from 5% at 300 K to ~20% at 473 K. In the DFT study (B3LYP/6-311G* level) it was shown that a $[Cm(H_2O)_9(H_2O)_{18}]^{3+}$ cluster with TTP coordination geometry and D_3 symmetry (first hydration shell) is more stable in the gas phase than is a cluster with D_{3h} symmetry.[8] However, upon inclusion of a conductor-like polarizable continuum medium (CPSM) solvent model the latter cluster (referred to as "structure B" in ref 8) was found to be more stable than the former ("structure A") by ~5 kcal/mol. In structure B, the special hydrogen bonding between the capping waters and the waters in the second hydration shell induces a separation in the prismatic (2.49 Å) and the capping (2.54 Å) Cm−O distances.

The $^6D'_{7/2} \rightarrow {}^8S'_{7/2}$ luminescence spectrum of Cm^{3+} is very sensitive to changes in the local structure. While the spectrum of the fully hydrated, unperturbed Cm^{3+} ion in aqueous solution gives rise to a single band at ~594 nm at room temperature, a change in its first coordination shell usually results in a red

* Corresponding author: phone, +49-724-7822389; fax, +49-724-7823927; e-mail, plr@ine.fzk.de.
† Forschungszentrum Karlsruhe.
‡ Lawrence Berkeley National Laboratory.

10.1021/jp808491k CCC: $40.75
Published on Web 12/08/2008

shift.[10,13] Hence, the room temperature ${}^6D'_{7/2} \rightarrow {}^8S'_{7/2}$ spectrum of the $[Cm(H_2O)_9]^{3+}$ ion with slightly distorted coordination TTP geometry in $[La(H_2O)_9]Cl_3 \cdot 15\text{-crown-}5 \cdot H_2O$ is similar to that of $Cm^{3+}(aq)$ at 20 °C, indicating similar local structures in aqueous solution and the solid hydrate.[13] On the other hand, the spectrum of $[Cm(H_2O)_8]^{3+}$ with a distorted bicapped trigonal prismatic geometry in $[Y(H_2O)_8]Cl_3 \cdot 15\text{-crown-}5$ is red-shifted by ~2.5 nm; this spectrum is comparable to that of $Cm^{3+}(aq)$ at 200 °C, thus suggesting an 8-fold-coordinated Cm^{3+} aqua species at elevated temperature.[13,14] Moreover, the ${}^8S'_{7/2} \rightarrow {}^6D'_{7/2}$ excitation spectrum of $Cm^{3+}(aq)$ at 20 °C resembles that of the $[Cm(H_2O)_9]^{3+}$ ion with C_{3h} symmetry in $[Y(H_2O)_9](CF_3SO_3)_3$,[2] while the excitation spectrum of the octahydrate is red-shifted and shows a different overall peak shape.[2] In these examples the differences in the spectra are solely caused by differences in the coordination geometries, which affect the local crystal field interactions. In all but cubic symmetries, the local crystal field interaction splits a $J = {}^7/_2$ multiplet into four Kramers doublets; hence the first excited state ${}^6D'_{7/2}$ multiplet is split into four levels (denoted here as A_{1-4}). Thus, for Cm^{3+} in $[Y(H_2O)_9](CF_3SO_3)_3$ and $[La(H_2O)_9]Cl_3 \cdot 15\text{-crown-}5 \cdot H_2O$ the A_1-A_4 splitting was determined as to be approximately 410 and 540 cm^{-1}, respectively,[2,13] while in $[Y(H_2O)_8]Cl_3 \cdot 15\text{-crown-}5$ it is significantly larger, ~660 cm^{-1}.[13,14] In comparison, the crystal-field splitting of the ground nominally ${}^8S'_{7/2}$ multiplet (which splits into four Kramers doublets denoted as Z_{1-4}) is much smaller. The total splitting of the ground state depends critically on the host structure; for example, it is 2 cm^{-1} in $LaCl_3$ (nine Cl ions in C_{3h} symmetry)[15,16] and 36 cm^{-1} in ThO_2 (eight oxygen ions, O_h symmetry),[17] although values in the range of 10−20 cm^{-1} are more common.[10] Nevertheless, these values are more than 1 order of magnitude larger than the corresponding values for Gd^{3+}, the $4f^7$ analogue of Cm^{3+} ($5f^7$). The larger ground-state splitting in Cm^{3+} is due primarily to the fact that its ground state (only ~78% ${}^8S_{7/2}$) has an admixture of many other LS states such as ${}^6P_{7/2}$ (~19%), induced by the relatively strong spin−orbit coupling.[10]

In this paper we determine the $5f^7$ electronic level structure of the ground and first excited multiplets of $[Cm(H_2O)_9]^{3+}$ ions incorporated into four different crystalline hosts. These nonaaqua species may be considered as structure units of the first hydration sphere of $Cm^{3+}(aq)$. Hence, the results presented here connect to the discussion about the hydration structure of An^{3+} ions in aqueous solution.[1−9] Although it is not possible to discern the individual levels of the ground multiplet for $Cm^{3+}(aq)$, we may, however, estimate an approximate value for the total splitting. High-resolution optical spectroscopic studies of $[Cm(H_2O)_9]^{3+}$ species incorporated into crystalline hosts at low temperature provide such information. As will be shown in this work, the total ground multiplet splitting is in the range of 6−8 cm^{-1} for nonahydrated Cm^{3+} in the rare-earth hosts $[M(H_2O)_9](CF_3SO_3)_3$ and $[M(H_2O)_9](C_2H_5SO_4)_3$. We believe that these relatively small values represent lower limits for a $[Cm(H_2O)_9]^{3+}$ ion, while slightly higher values are to be expected for distorted 9-fold coordination geometries. However, a surprisingly large value of 35 cm^{-1} was obtained for $[Cm(H_2O)_8]^{3+}$ in $[Y(H_2O)_8]Cl_3 \cdot 15\text{-crown-}5$;[14] thus, it was thought that this large value was caused by the distorted bicapped trigonal prismatic coordination geometry and/or a fairly short Cm−O bond distance. Apart from that study and a recent communication presenting the room temperature ${}^6D'_{7/2} \rightarrow {}^8S'_{7/2}$ emission and ${}^8S'_{7/2} \rightarrow {}^6D'_{7/2}$ excitation spectra of Cm^{3+} in $[Y(H_2O)_9](CF_3SO_3)_3$,[2] no other papers presenting the ground- and excited-state electronic structures of Cm^{3+} in crystalline hydrates have been published.[18]

Here, we use high-resolution TRLFS to derive the electronic level structure of the ground ${}^8S'_{7/2}$ multiplet and the excited state ${}^6D'_{7/2}$ multiplet of $[Cm(H_2O)_9]^{3+}$ ions diluted into the crystal lattices of nonahydrated rare-earth trifluoromethanesulfonate (triflate) and ethyl sulfate salts, $[La(H_2O)_9](CF_3SO_3)_3$ (**1**), $[Y(H_2O)_9](CF_3SO_3)_3$ (**2**), and $[Y(H_2O)_9](C_2H_5SO_4)_3$ (**3**).[19a,20] Characteristic of these three isotypic series is the regular TTP coordination geometry of the nonahydrated cations with C_{3h} symmetry. As an isotypic series the hydrated rare-earth triflate salts comprise all Ln^{3+} ions, Y^{3+} and Sc^{3+},[19bc,21] and the recently published crystal structures of the actinide ion analogues Pu^{3+}, Am^{3+}, and Cm^{3+}.[22,1,2] Detailed descriptions of the crystal structures of the two isotypic series are given elsewhere[19,20,23] and will be briefly reviewed here. The $[La(H_2O)_9]Cl_3 \cdot 15\text{-crown-}5 \cdot H_2O$ (**4**) salt has relatively low crystal symmetry and the coordination geometry of the hydrated lanthanum ion is a distorted TTP. Its crystal structure is reported here; the compound is further used as host for Cm^{3+} as it mimics well the probable local structure of the Cm^{3+} aqua ion.

Experimental Section

Sample Preparation. High-purity (99.99%) La_2O_3 and Y_2O_3 were used in order to avoid luminescence from impurity ions, e.g., Eu^{3+}. All compounds were crystallized from their respective aqueous solutions by slow evaporation of the excess water at room temperature. The preparation procedures of the solutions and the crystal compounds of **1**−**4** are described elsewhere.[19,20,23] Parts of the crystals were used for X-ray diffraction for determination of unit cell parameters, which were found to be in agreement with published data,[19,20,23] and chemical analysis (i.e., EDTA titration (xylene orange indicator) and cation exchange (Dowex 50W-X8, H^+-form) for checking the M^{3+} and anion contents, respectively). The other part of the crystalline material was recrystallized by addition of Cm^{3+} stock solution (i.e., 50 μmol/L Cm^{3+} in 0.1 mol/L aqueous $HClO_4$) to give a final Cm^{3+} concentration of less than 1 ppm.[24] Deuterated samples were prepared by dissolving the solids in D_2O, evaporating by gently heating the solutions under a stream of argon to dryness, and dissolution in D_2O. This procedure was repeated three to four times to ensure complete H/D exchange. Crystallization of these solutions was performed in closed vessels placed in an argon-filled glovebox.

Crystallography. Single-crystal X-ray diffraction data for **4** were collected using a Bruker SMART diffractometer with a CCD area detector and Mo Kα radiation ($\lambda = 0.7107$ Å). Data reduction, empirical absorption correction, and structure determination (direct methods) were performed using Bruker standard software.[25] All non-hydrogen atoms were refined with anisotropic displacement parameters.[26] The hydrogen atoms belonging to the crown ether were added at calculated positions and refined using a riding model, while those of the water molecules were located from the residual electron density map. The crown ether molecule is disordered at room temperature; this is accounted for by large thermal ellipsoids of its carbon and oxygen atoms. The molecular structures depicted in Figure 1 were drawn using the program DIAMOND.[27]

TRLFS. All samples used were polycrystalline (powder-like); this reduces orientation effects of the fluorescence emission relative to the linearly polarized laser beam. The samples were mounted on an in-house constructed copper sample holder, attached to the cold head of the cryostat (Cryodyne Cryocooler model 22C, compressor 8200, CTI-Cryogenics, USA). An XeCl-excimer laser (Lambda Physics, EMG, 308 nm) pumped dye-laser (Lambda Scanmate; pulse width 20 ns, spectral width 0.2

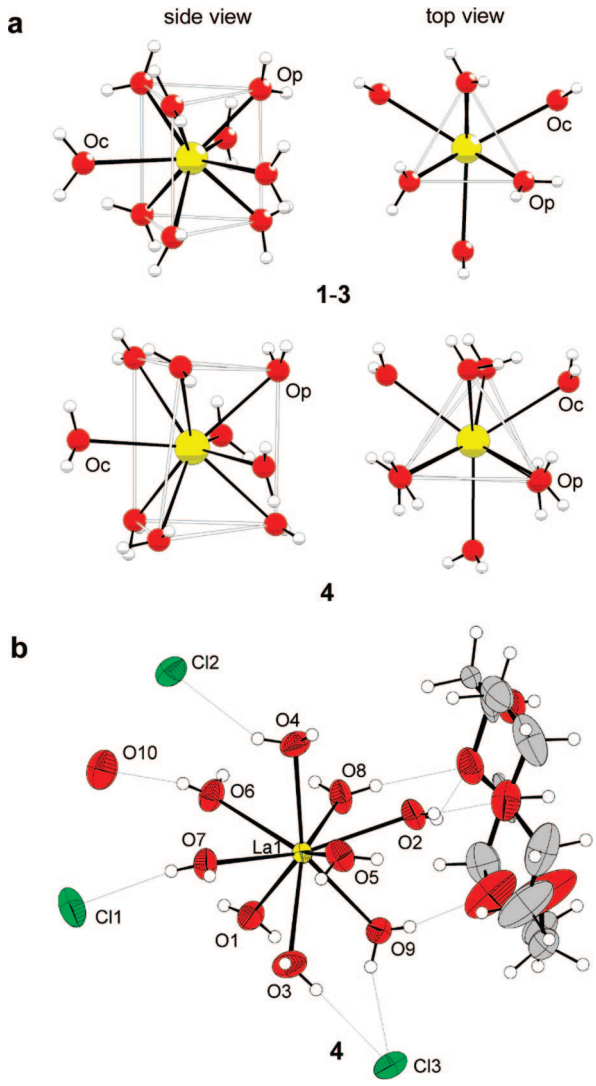

Figure 1. (a) Local structures around the $[M(H_2O)_9]^{3+}$ cations in the crystal hosts of **1**−**4**, showing their tricapped trigonal prismatic (TTP) coordination geometries as viewed from the side and from the top. Note the slight rotation of the capping oxygens (O_c) in the equatorial plane in **1**−**3**, giving rise to C_{3h} point symmetry. The point symmetry in **4** is approximately C_2. The molecular structures depicted for **1**−**3** are obtained from the crystal structure data of **2** from ref 19a. (b) Molecular structures of the $[La(H_2O)_9]^{3+}$ cation species in **4**, showing parts of its hydrogen bonding to the crown ether, chloride ions, and the lattice water molecule. The thermal ellipsoids are drawn at the 40% probably level for all non-hydrogen atoms. The La−O bond distances (Å) are as follows: La1−O1, 2.536(3); La1−O4, 2.543(4); La1−O2, 2.545(3); La1−O9, 2.545(4); La1−O6, 2.555(4); La1−O7, 2.557(3); La1−O8, 2.558(4); La1−O5, 2.574(5); La1−O3, 2.629(4).

cm^{-1}, wavelength accuracy 0.5 cm^{-1}) was used. All emission spectra not requiring high-resolution detection, including the fluorescence emission detection of the excitation spectra, were recorded by an optical multichannel analyzer, consisting of a Czerny-Turner polychromator (Jobin Yvon, HR 320) with three gratings, 300, 600, and 1200 lines/mm, and a gated, intensified photodiode array (Spectroscopy Instruments, ST 180, IRY 700G). To measure the decay time of the fluorescence emission for the H_2O (D_2O) crystalline hydrates, the intensifier was opened for typically 1 (10) ms at delay times of 1−400 (1−10000) μs between laser excitation and detection in steps of 5 (100) μs. For these measurements and for the low-resolution emission spectra, the excitation wavelength was set to about 25200 cm^{-1} using the laser dye QUI. This excitation wavelength is preferred as it corresponds to the F-state ($^6I_{17/2}$, $^6I_{11/2}$) of Cm^{3+}, which has the highest absorptivity and therefore gives rise to maximum emission intensity at the metastable A state ($^6D'_{7/2}$ multiplet).

Excitation spectra were measured with fixed delay time and gate width at 10 μs and 3.5 ms, respectively. For each excitation wavelength the full emission spectrum was recorded; in this way our excitation measurements differ from other similar studies, in which a single emission wavelength is selected using a monochromator (see, e.g., refs 15 and 16). The step size of the excitation wavelength was adapted to typically 20 cm^{-1} for the low-resolution excitation spectra at room temperature and 0.06−0.2 cm^{-1} for the high-resolution spectra at 20 K. Calibration of the dye laser excitation wavelengths (in air) was performed with a wavelength meter, which has a precision of 10^{-7}. To cover the $^6D'_{7/2}$ multiplet in the excitation spectra, the dye laser was scanned from about 16660 to 17860 cm^{-1} using Coumarin 153. The spectral resolution of the Czerny-Turner polychromator was determined to be about 12 cm^{-1} at 600 nm.

High-resolution $^6D'_{7/2}(A_1) \rightarrow {}^8S'_{7/2}$ emission spectra were recorded at 20 K using an ANDOR iStar camera system with a holographic 2400 lines/mm grating. Direct excitation into the resonant A_1 level was not possible due to incomplete discrimination of the more intense laser scatter from the weaker emission of Cm^{3+}; therefore, emission from the A_1 level by excitation into the F state was measured. (Note, however, that direct excitation into A_1 was recently performed for compound **5** using an Echelle spectrometer; see ref 14). The Grams32 software package (Galactic Industries Inc.) was used for peak deconvolution and curve fitting of the emission and excitation spectra (Figure 4 and Figure S1 in the Supporting Information).

Results

Host Structures. Figure 1a compares the two types of TTP coordination geometries of the $[M(H_2O)_9]^{3+}$ ions in the crystal hosts of **1**−**4**; the compositions and coordination geometry data for these hosts are listed in Table 1. The structures of the cation species in the triflate (**1** and **2**) and ethyl sulfate (**3**) salts are nearly indistinguishable and therefore are represented with one structure. The coordination polyhedron of **4** is a distorted TTP with approximately C_2 point symmetry. In **1**−**3** the hydrated cations comprise six prismatic oxygen atoms (O_p) located at the corners of the trigonal prism at shorter M−O distances and three capping oxygens atoms (O_c) in the equatorial plane at longer distances. The differences between the M−O_p and M−O_c distances increase across the lanthanide (La−Lu) series. These changes are usually expressed by means of the M−O_c/M−O_p ratio. This ratio increases with decreasing metal ionic radius due to the increasing steric crowding between the water ligands.[19,20] The structure of the hydrogen bond network between the $[M(H_2O)_9]^{3+}$ cations and the anions is also crucial for the size and the shape of the cationic species. Indeed, the composition of the hydrogen bond networks in the triflate and ethyl sulfate series induces C_{3h} point symmetry (deviation from D_{3h} symmetry by a slight rotation of the capping oxygens in the equatorial plane) at the metal centers and a relatively large difference between the M−O_c and M−O_p distances. An important structural difference that distinguishes the triflate and ethyl sulfate series from the well-known bromate series is the orientation of the capping waters. In the former two series, the hydrogen atoms of the capping waters are located above and below the equatorial plane, while in the latter series they are located in the plane.[19,20,28]

TABLE 1: Compositions and Coordination Geometry Data for the Host Compounds 1−5

host compound	geometry (symmetry)	bond distances r(Ln−O)/Å
$[Cm(H_2O)_9](CF_3SO_3)_3$[a]	TTP (C_{3h})	6 × 2.45, 3 × 2.57
1 $[La(H_2O)_9](CF_3SO_3)_3$[b]	TTP (C_{3h})	6 × 2.52, 3 × 2.62
2 $[Y(H_2O)_9](CF_3SO_3)_3$[b]	TTP (C_{3h})	6 × 2.34, 3 × 2.53
3 $[Y(H_2O)_9](C_2H_5SO_4)_3$[c]	TTP (C_{3h})	6 × 2.37, 3 × 2.52
4 $[La(H_2O)_9]Cl_3 \cdot 15C5 \cdot H_2O$[d]	TTP($\sim C_2$)	2.54−2.63
5 $[Y(H_2O)_8]Cl_3 \cdot 15C5$[e]	BTP($\sim C_2$)	2.32−2.43

[a] Reference 2. [b] Reference 19a. [c] Reference 20a. [d] This study. [e] Reference 14.

Figure 1b shows the local structure about the $[La(H_2O)_9]^{3+}$ ion in the crystal structure of **4** at 295 K, including parts of its hydrogen bonds to the crown ether, the chloride ions, and the lattice water. The crown ether molecule is affected by disorder, even though it accepts four hydrogen bonds from one side and two from the other side. In contrast, no such disorder occurs for $[La(H_2O)_9]^{3+}$, indicating some flexibility in the hydrogen bond network between the water ligands and the crown ether, the chloride ions, and the lattice water. Since this water molecule accepts one hydrogen bond from a "first shell" water (O6···O10 = 2.687(6) Å), it may be recognized as a "second coordination shell" water in the $[La(H_2O)_9]^{3+} \cdot H_2O$ moiety. The La−O bond distances are in the range 2.54−2.63 Å.

The mean Cm−O distances in the $[Cm(H_2O)_9]^{3+}$ species are predicted to be ∼0.07 Å shorter than the mean La−O distance in **1** and **4** and ∼0.08 Å longer than the mean Y−O distance in **2** and **3**, consistent with the differences in the ionic radii between Cm^{3+} (1.094 Å, eight-coordination)[29] and the host metal ions La^{3+} (1.160 Å) and Y^{3+} (1.015 Å).[30] Nevertheless, minor distortions of the coordination geometry are expected to occur as Cm^{3+} replaces a larger or a smaller host ion than itself. This size mismatch may thus induce either a negative or a positive lattice pressure on Cm^{3+} thereby causing changes in the local crystal field (see below).

Room Temperature Emission and Excitation Spectra. Figure 2 compares the room temperature $^6D'_{7/2} \rightarrow {}^8S'_{7/2}$ emission and $^8S'_{7/2} \rightarrow {}^6D'_{7/2}$ excitation spectra of the $[Cm(H_2O)_9]^{3+}$ species in **1**−**4**. Since the ground-state splitting of the $^8S'_{7/2}$ multiplet is relatively small, it does not affect the spectra at room temperature appreciably. The vertical dashed line at 16840 cm^{-1} corresponds to the peak maximum of the emission spectrum of Cm^{3+}(aq). The emission spectra of Cm^{3+} in the triflate (**1**−**2**) and ethyl sulfate (**3**) hosts display similar Lorentzian bands with peak maxima at around 16900 cm^{-1}. These main bands result from the emissions from the close lying first (A_1) and second (A_2) levels of the metastable $^6D'_{7/2}$ multiplet to the $^8S'_{7/2}$ ground multiplet, whereas the very weak features at higher energies are due to emission from the thermally populated third (A_3) and fourth (A_4) levels. The excitation spectra are more complex. Apart from the major A_1-A_2 band whose shape and position match well the corresponding emission band, they also contain two broader, overlapping A_3 and A_4 bands of lower intensities at ∼17100 and ∼17300 cm^{-1}. In order to derive spectroscopic parameters for these levels, each of the emission and excitation spectra is curve-fitted with three Lorentzian functions, which describe well the A_1-A_2, A_3, and A_4 component bands of the $^6D'_{7/2}$ multiplet (see Figure S1 and Table S1 in the Supporting Information). Evidently, the main A_1-A_2 band can be fit with one single Lorentzian band, even though it originates from two different transitions, $^6D'_{7/2}(A_1, A_2) \rightarrow {}^8S'_{7/2}$ and $^8S'_{7/2} \rightarrow {}^6D'_{7/2}(A_1, A_2)$ in the emission and excitation spectra, respectively. The broadening of this band owing to the relatively small energy separation between the levels A_1 and A_2, the crystal-field splitting of the ground state, and the temperature-induced dynamical distortions of the CmO_9 polyhedra, contribute to make these two bands appear as one symmetric band at room temperature. However, the peak position and the width of this band depend on the crystal host; thus, slight red shifts and a broadening of the band are observed in **2** compared to that of **1**. On the other hand, the positions of the A_3 (∼17100 cm^{-1}) and A_4 (∼17300 cm^{-1}) bands seem to be relatively independent of the host (cf. Table 2 and Figure 2 and the Supporting Information for tabulated fit parameters). The emission and excitation spectra of **4** clearly display the A_1 and A_2 component bands; their peak positions are in good agreement with those of Cm^{3+}(aq) at room temperature.[2,13]

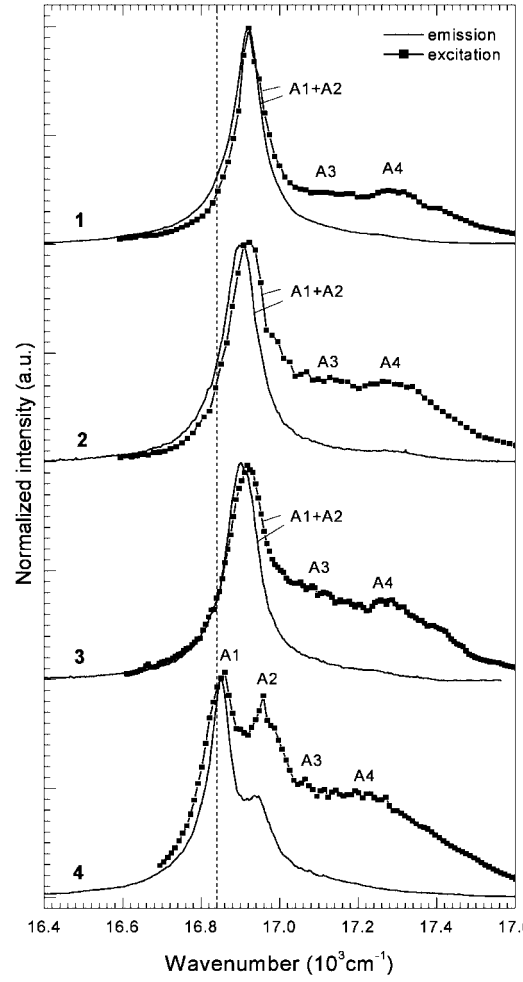

Figure 2. Room temperature $^6D'_{7/2} \rightarrow {}^8S'_{7/2}$ emission ($\lambda_{ex} \approx$ 397 nm, 25190 cm^{-1}) and $^8S'_{7/2} \rightarrow {}^6D'_{7/2}$ excitation spectra of $[Cm(H_2O)_9]^{3+}$ in **1**−**4**. The vertical dashed line represents the peak maximum of the emission spectrum of Cm^{3+}(aq).

Low Temperature Spectra. (a) Triflate and Ethyl Sulfate Hosts. With decreasing temperature the bandwidths (fwhm) of the main transitions decrease from about 100 cm^{-1} at 293 K to about 0.5−1 cm^{-1} at 20 K, accompanied by a substantial (8- to

TABLE 2: Energy (in cm^{-1}) of Identified Crystal-Field Levels of Kramers Doublets of the $^8S'_{7/2}$ Ground State (Z_n) and the $^6D'_{7/2}$ Excited State (A_n) in the Excitation Spectra of Cm^{3+} in 1−5

		1	2	3	4	5[a]
$^8S'_{7/2}$	Z_1	0.0[b]	0.0[b]	0.00[c]	[g]	0.0
	Z_2	3.4[b]	3.4[b]	3.34[c]	[g]	9.6
	Z_3	4.3[b]	4.5[b]	4.06[c]	[g]	18.5
	Z_4	8.0[b]	6.0[b]	7.67[c]	[g]	34.9
$^6D'_{7/2}$	A_1	16926.5[b]	16905.4[b]	16906.77[c]	16865[d]	16804.5
	A_2	16965.4[b]	16962.5[b]	16960.13[c]	16988[d]	16915
	A_3	17068[e]	17067[e]	17075[e]	17124[e]	17054
	A_4	17302[e]	17296[e]	17300[e]	17295[e]	17461
	cg[h]	17065[f]	17058[f]	17060[f]	17068[f]	17059
	Δ	376[d]	391[d]	393[d]	430[d]	656

[a] From reference 14. [b] ±0.2 cm^{-1}. [c] ±0.06 cm^{-1}. [d] ±5 cm^{-1}. [e] ±30 cm^{-1}. [f] ±20 cm^{-1}. [g] Not resolved due to inhomogeneous line broadening. [h] Center of gravity (arithmetic mean value of A_{1-4}).

10-fold) increase of the peak intensity (cf. Figure 3 and Figure S2 in the Supporting Information). The band narrowing with decreasing temperature results in partly to fully resolved A_1 and A_2 bands with peak maxima at (A_1/A_2) 16927/16965, 16905/16962, and 16907/16960 cm^{-1} for **1**−**3**, respectively. Since the thermal population of the A_2 level decreases with decreasing temperature, the spectra at 20 K are almost entirely due to emission from A_1. A quite different situation takes place in the low temperature excitation spectra. Whereas with decreasing temperature the A_1-A_2 excitation band gains intensity, narrows, and splits up into two component bands, the A_3 and A_4 bands lose intensity. Thus, at 20 K the spectra are dominated by the very narrow A_1 and A_2 resonant bands whose positions coincide with those of the emission spectra (cf. Figure 3 and Table 2). Similarly, for Cm^{3+} in $LaCl_3$ only the A_1 (16815 cm^{-1}) and A_2 (16876 cm^{-1}) bands were observed in the excitation spectrum at 4.2 K.[16,31]

Several weak bands observed at the low energy side of the $^6D'_{7/2}(A_1) \rightarrow {}^8S'_{7/2}$ electronic transition in the low temperature emission spectra and at the high energy side of the $^8S'_{7/2} \rightarrow {}^6D'_{7/2}(A_1, A_2)$ transitions in the excitation spectra are assigned to vibronic transitions (see insets to Figure 3). These vibronic side bands (VSB) result from the interactions between the electronic transition and the various phonon modes localized at the Cm^{3+} ion. The vibronic-excitation spectra are more complex than the vibronic-emission spectra, since the excitations into the $^6D'_{7/2}(A_1)$ and $^6D'_{7/2}(A_2)$ electronic states generate two superimposed vibronic spectra, but shifted by approximately 39, 57, and 53 cm^{-1} in **1**, **2**, and **3**, respectively. Yet, for the three hosts the vibronic spectra in excitation are rather similar to those in emission, indicating that the vibronic intensity at the $^8S'_{7/2} \rightarrow {}^6D'_{7/2}(A_2)$ transition is relatively weak.

Although the primary $^6D'_{7/2}(A_1) \rightarrow {}^8S'_{7/2}$ and $^8S'_{7/2} \rightarrow {}^6D'_{7/2}(A_{1,2})$ transitions in the low-temperature emission and excitation spectra of **1**−**3** appear as single lines in Figure 3, each should be split into four lines reflecting the $^8S'_{7/2}$ ground-state splitting. The high-resolution excitation spectra in Figure 4a show that the transitions involving the A_1 and A_2 levels are split into three fairly sharp lines for **1** and **2** and four lines for **3**, while due to the lower resolution in the emission spectra only three lines involving the (four) transitions from the A_1 level are clearly observed (Figure 4a). The fourth expected line is not resolved in the excitation spectra of **1** and **2**, while the exceptionally high quality of the spectrum of **3** enables the resolution of all four transitions. We assign the highest energy bands in the two quartets to the transitions from the ground-state level, Z_1, to the A_1 and A_2 crystal-field levels, and the second, third, and fourth bands are assigned to transitions Z_2, Z_3, and Z_4 to A_1 and A_2, respectively. In order to resolve the bands arising from transitions from Z_2 and Z_3 to A_1 and A_2 in **1** and **2**, curve fitting of their excitation spectra was performed. The curve-fitted spectra with obtained peak positions are shown in Figure 4b,c. The peak-to-peak energy differences in the two quartets at A_1 and A_2 correspond to the ground-state splitting: (in cm^{-1}) **1** (A_1, 0.0, 3.4, 4.3, 8.0; A_2, 0.0, 3.4, 4.3, 8.0), **2** (A_1, 0.0, 3.4, 4.4, 6.0; A_2, 0.0, 3.4, 4.9, 5.9), and **3** (A_1, 0.00, 3.37, 4.09, 7.71; A_2, 0.00, 3.31, 4.01, 7.62). Interestingly, the relative intensities of the lines at A_1 differ significantly from those at A_2 (e.g., in **3** A_1 (1.00, 0.09, 0.07, 0.13) and A_2 (0.08, 0.23, 0.19, 0.34)), showing that the transition probabilities between the sublevels of the ground-state and the A_1 and A_2 crystal-field levels of the excited state are very different. It is noteworthy that the total ground-state splitting is larger while the splitting between the A_1 and A_2 crystal-field levels is smaller in **1** (8.0, 38.9 cm^{-1}) than those in **2** (6.0, 57.0 cm^{-1}), while the corresponding values in **3** (7.7, 53.4 cm^{-1}) are comparable to those of **2**.

Since the transitions involving the A_1 and A_2 levels show the same 4-fold splitting pattern, it is likely that each of the resonance bands originate from a transition arising from the ground-state multiplet of Cm^{3+} ions located in one unique crystallographic site rather than four different sites. This is confirmed by high-resolution emission spectra, where excitations into either of the four resonance bands of A_2 yield virtually identical emission spectra, with the same splitting and peak positions as the excitation spectra (spectra not shown). High-resolution emission spectra of **1**−**3** were also recorded at different delay times between 1 and 300 μs (see Figure S2 of the Supporting Information). Each of these spectra is virtually identical with those depicted in Figure 4a, again showing that this apparent 3-fold splitting originate from the splitting of the ground state of Cm^{3+} ions situated in one unique crystal site.

(b) $[La(H_2O)_9]Cl_3 \cdot$15-crown-5$\cdot H_2O$ (4) Host. The peak maxima and the peak shapes of the room temperature emission and excitation spectra of **4** are similar to those of Cm^{3+}(aq). Hence, this host appears to mimic structure and the crystal-field strength around the hydrated Cm^{3+} ion in aqueous solution (see below). However, as can be seen in the low temperature excitation spectrum in Figure 5, the A_1 and A_2 bands are rather broad and, due to inhomogeneous line broadening, the individual ground states are not resolved.

Luminescence Lifetime. The luminescent decays of the $^6D'_{7/2}$ excited state of **1**−**4** are monoexponential at room temperature, confirming that $[Cm(H_2O)_9]^{3+}$ species are incorporated into the metal ion sites of the crystal hosts. The deduced luminescence lifetimes, τ_{obs} ($=k_{obs}^{-1}$; k_{obs} is the decay rate constant) are listed in Table 3. The lifetimes in **1** and **2** (both 63 ± 2 μs) are comparable to those of $[Cm(H_2O)_9](CF_3SO_3)_3$ (66 ± 2 μs)[2] and Cm^{3+}(aq) at 293 K (65 ± 2 μs) but shorter than those in **3** and **4** (both 74 ± 2 μs). Note that for some of the compounds the lifetimes may be slightly longer at 20 K. In comparison, the lifetimes of the deuterated analogues are considerably longer (τ_{obs} = (**1**) 1220 ± 20, (**2**) 1550 ± 20, and (Cm^{3+}(aq)) 1370 ± 20 μs; the shorter lifetime in **1** is most likely due to impurities with H_2O; the deuterated salts of **3** and **4** were not studied).

Discussion

Crystal-Field Splitting vs Crystal-Field Strength. The identified crystal-field levels of the $^8S'_{7/2}$ (Z_1-Z_4) and $^6D'_{7/2}$ (A_1-A_4) multiplets of the $[Cm(H_2O)_9]^{3+}$ ions in **1**−**4** are

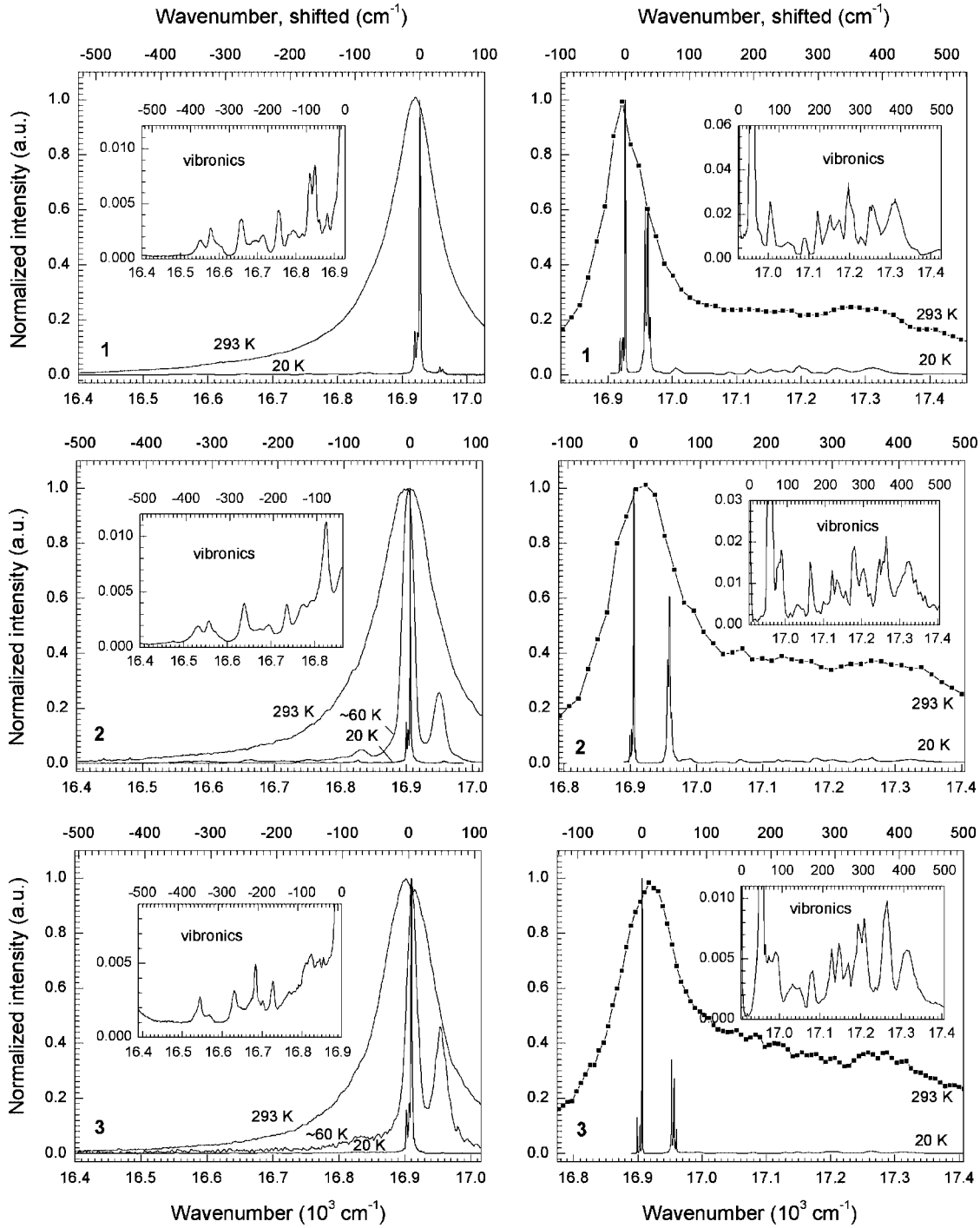

Figure 3. Intensity normalized (left) $^6D'_{7/2} \rightarrow {}^8S'_{7/2}$ emission ($\lambda_{ex} \approx 25190$ cm^{-1}) and (right) $^8S'_{7/2} \rightarrow {}^6D'_{7/2}$ excitation spectra of $[Cm(H_2O)_9]^{3+}$ in **1**−**3** at 293 and 20 K (the emission spectra at ∼60 K are also shown). The shifted wavenumber scales (top) have shifts of 16926.5, 16905.4, and 16906.77 cm^{-1} for **1**−**3**, respectively, relative to the absolute wavenumber scales (bottom), corresponding to the energies of the $^6D'_{7/2}(A_1)$−$^8S'_{7/2}(Z_1)$ transitions (zero-phonon lines) in the high-resolution emission and excitation spectra in Figure 4a. The insets show the vibronic side bands (in the region 0−500 cm^{-1}), which are associated with the respective zero-phonon lines in the emission and excitation spectra at 20 K.

listed in Table 2 and depicted in Figure 6; the corresponding levels for the octahydrated Cm^{3+} ion in $[Y(H_2O)_8]Cl_3 \cdot 15$-crown-5 (**5**) are included for comparison. Also indicated are the centers of gravity of the $^6D'_{7/2}$ multiplets, all of which appear at ∼17060 cm^{-1} despite the fact that individual A_1−A_4 levels may differ considerably. These approximately constant centers of gravity of the $^6D'_{7/2}$ multiplets is indicative that the free ion parameters for the Cm^{3+} ion in the various host crystals do not change significantly. Among these crystal-field levels, A_1 is most sensitive to differences in the coordination geometry. Its energy position decreases slightly on going from **1** (16927 cm^{-1}) to **2** (16905 cm^{-1}) ≈ **3** (16907 cm^{-1}) and drops readily in **4** (16864 cm^{-1}). In comparison, the A_2, A_3, and A_4 levels show somewhat smaller variations in energy, although the positions of the latter two are not well defined in the excitation spectra (cf. Figures 2, 3, 5, and 6). This means that the total splitting (Δ, in cm^{-1}) of the $^6D'_{7/2}$ multiplet increases with decreasing energy of A_1 in the same order: **1** (376 cm^{-1}), **2** (391 cm^{-1}) ≈ **3** (393 cm^{-1}), **4** (430 cm^{-1}). In comparison, the splitting in the octahydrate (**5**) is considerably larger (656 cm^{-1});[14] cf. Table 2 and Figure 6.

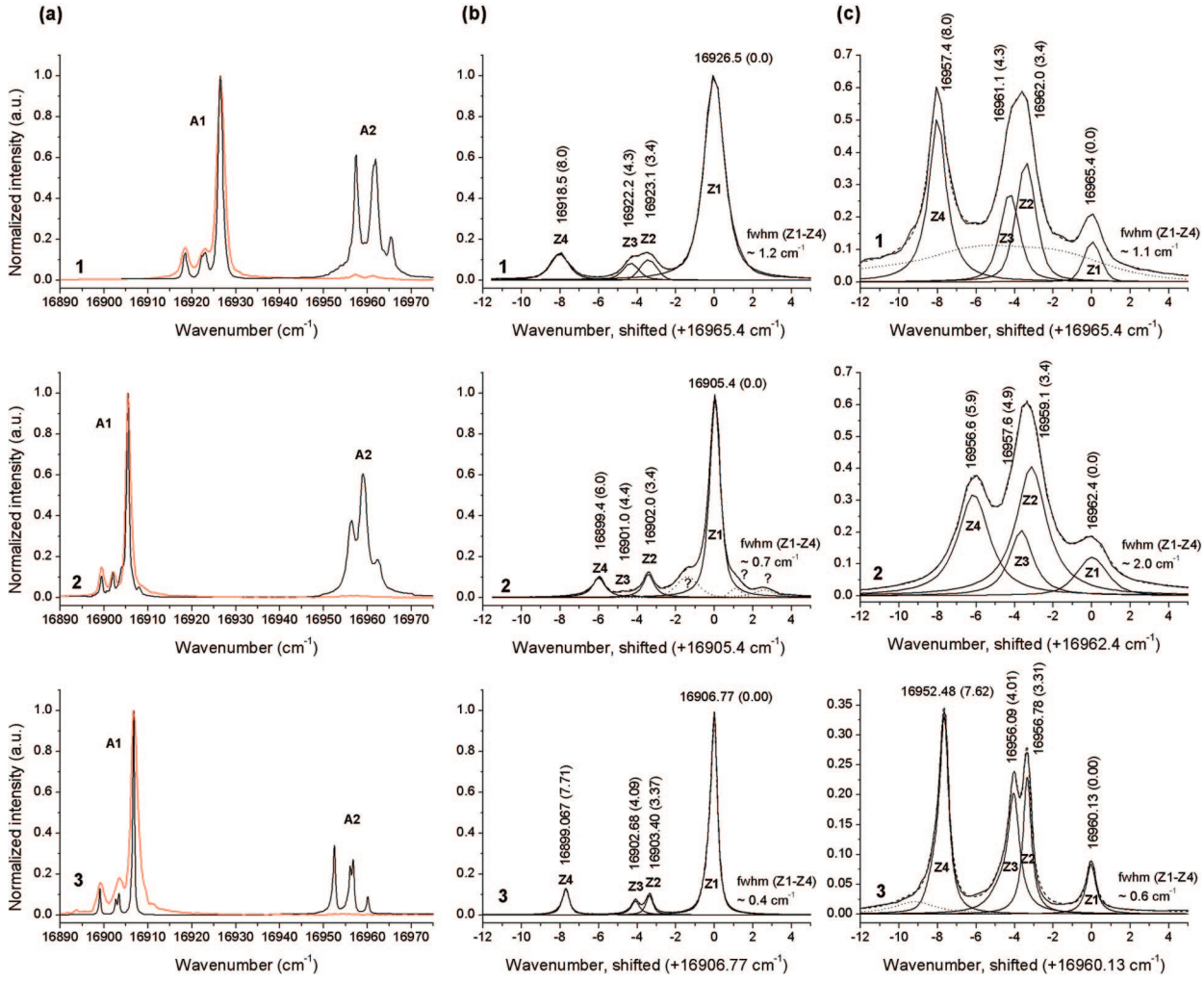

Figure 4. (a) High-resolution $^8S'_{7/2}(Z_{1-4}) \rightarrow {}^6D'_{7/2}(A_{1,2})$ excitation (black lines) and $^6D'_{7/2}(A_1) \rightarrow {}^8S'_{7/2}(Z_{1-4})$ emission ($\lambda_{ex} \approx 25190$ cm^{-1}) (red lines) spectra of $[Cm(H_2O)_9]^{3+}$ in **1**−**3** at 20 K. Note that the emission spectra are affected by additional instrumental broadening, which is why only three lines are observed in the emission spectrum of **3**, even though its excitation spectrum shows four lines. (b and c) Curve-fitted excitation spectra at the A_1 and A_2 levels, respectively. The ground-state splitting is modeled by fitting four Lorentzian bands (denoted as Z_n) to the experimental data (solid lines). The dotted lines at the A_2 levels account for additional intensities which are most likely of vibronic origin. For the sake of comparison, in (b) and (c) the wavenumber scales are shifted by the energy corresponding to the transition from the lowest ground-state level, Z_1.

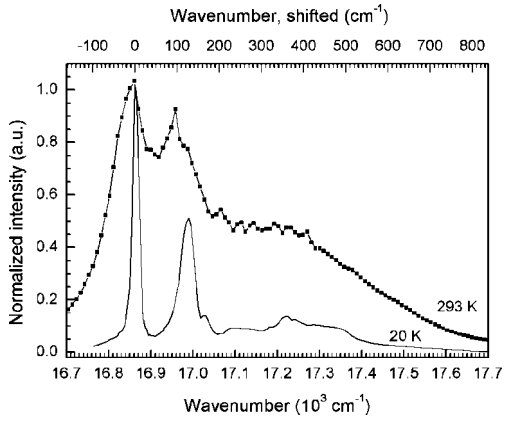

Figure 5. Intensity normalized $^8S'_{7/2} \rightarrow {}^6D'_{7/2}$ excitation spectra of $[Cm(H_2O)_9]^{3+}$ in **4** at 293 and 20 K. The shifted wavenumber scale (top) has a shift of 16860 cm^{-1} relative to the absolute wavenumber scale (bottom).

The degree of splitting of the $^6D'_{7/2}$ multiplets in these nona- and octahydrates hydrates correlates with the coordination geometry and the strength of the local crystal field. For 4f and 5f ions it is known that the magnitude of the splittings of their respective multiplets depends on factors such as the type of ligand, the metal−ligand bond lengths, and the coordination geometry.[10] A comparison of different Eu(III) compounds showed that ideal (D_{3h}) or distorted (C_{3h}, D_3) TTP polyhedra result in particularly weak crystal fields and hence small crystal-field splittings.[32] Similarly, we obtain relatively small crystal-field splittings for the $^6D'_{7/2}$ and $^8S'_{7/2}$ multiplets for **1**−**3**, in which the metal ions feature regular TTP geometries (C_{3h} symmetry). However, the total splitting of the $^6D'_{7/2}$ multiplet is slightly smaller in the lanthanum triflate host than in the yttrium triflate host. This may be understood in terms of "internal

TABLE 3: Luminescence Lifetimes (in μs) at the $^6D'_{7/2}$ Level of $[Cm(H_2O)_{8-9}]^{3+}$ and $[Cm(D_2O)_{8-9}]^{3+}$ Ions in 1−5 at 293 and 20 K[a]

	τ_{H_2O} (293 K)	τ_{H_2O} (20 K)	τ_{D_2O} (293 K)
1	63	66	1220
2	63	66	1550
3	74	70	
4	74	74	
5[b]	68	69	

[a] Estimated errors are ±2 and ±20 μs for the hosts with H_2O and D_2O ligands, respectively. [b] From ref 14.

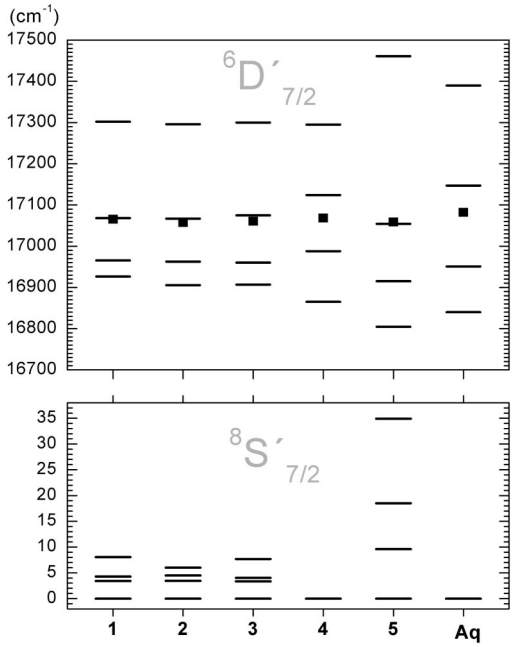

Figure 6. Comparison of $^8S'_{7/2}$ and $^6D'_{7/2}$ crystal-field energy levels of $[Cm(H_2O)_9]^{3+}$ ions in **1**−**4**, $[Cm(H_2O)_8]^{3+}$ ions in **5**,[14] and Cm^{3+}(aq) at 293 K.[13] The ground-state levels in **4** are not resolved. The center of gravity (■) of the $^6D'_{7/2}$ multiplet (arithmetic mean value of A_{1-4}) is also shown.

pressures", since with the replacement of La^{3+} by Cm^{3+} in **1** the dopant ion (Cm^{3+}) finds itself in a larger unit cell volume than it does in the neat compound $[Cm(H_2O)_9](CF_3SO_3)_3$. This excess volume would produce a negative internal pressure and a weaker crystal field compared to the neat salt. Hence, the smaller volume in **2** would produce a positive internal pressure which increases the crystal-field strength on Cm^{3+} by slightly compressing its coordination geometry. On the other hand, the ground-state splitting in **1** and **2** show the reverse trend, with a larger splitting in the former (see Table 2).

The crystal-field strength experienced by Cm^{3+} in these hosts may be estimated using a previously established linear correlation between the total ground $^8S'_{7/2}$ state splitting and the scalar crystal-field strength parameter (N_v').[33,34] For example, a relatively small N_v' value of 628 cm^{-1} was deduced for Cm^{3+} in $LaCl_3$ (C_{3h} symmetry), in which the ground-state splitting is very small, 2 cm^{-1}, and a rather large N_v' value of 2953 cm^{-1} in ThO_2 (O_h symmetry) where the splitting is large, 36 cm^{-1}.[16,10] With this linear correlation and the total ground-state splittings from Table 2, the estimated N_v' values for $[Cm(H_2O)_9]^{3+}$ in **1**−**3** are obtained as 1100, 1000, and 1080, respectively. These values are notably smaller than the estimated N_v' value for $[Cm(H_2O)_8]^{3+}$ in **5**, 2800 cm^{-1}. In comparison, for Eu^{3+} in $[Eu(H_2O)_9](C_2H_5SO_4)_3$ $N_v' \approx 280$ cm^{-1},[35] which is about four times smaller than the corresponding value for Cm^{3+} in **3**. This may be compared with earlier estimates showing that N_v' of an An^{3+} ion is about twice the value of a Ln^{3+} ion in a given host.[10]

Luminescence Quenching. It is well-known that the luminescence lifetime of the $^6D'_{7/2}$ excited state for a hydrated Cm^{3+} ion is greatly reduced by coupling with the OH overtones of the water ligands such that the luminescence decay rate constant increases proportionally with the number of water (n) ligands and their individual decay rate constants (k_{H_2O})[36,37]

$$\tau(H_2O)^{-1} = k_{obs}(H_2O) = k_r + nk_{H_2O} + C$$

where the constant C contains various nonradiative decay constants not originating from H_2O. In deuterated samples, because of the comparatively inefficient coupling with D_2O, $k_{obs}(D_2O)$ may only be slightly larger than the radiative decay constant, k_r; e.g., for **2** $k_{obs}(H_2O) = 15.9 \pm 0.5$ ms^{-1} at 293 K, while $k_{obs}(D_2O) = 0.645 \pm 0.010$ ms^{-1} ($\approx k_r$).[38] Therefore, since all four hosts incorporate $[Cm(H_2O)_9]^{3+}$ species and since the luminescence is quenched primarily by the (nine) H_2O ligands, it is somewhat surprising that the lifetimes of **3** (74 ± 2 μs) and **4** (74 ± 2 μs) are significantly longer than those of **1** (63 ± 2 μs) and **2** (63 ± 2 μs) and that of Cm^{3+}(aq) at 293 K (65 ± 2 μs). These lifetimes are slightly longer and shorter, respectively, than the "predicted" lifetime for nonahydrated Cm^{3+} (66 ± 3 μs), as calculated from the empirical equation ($n_{H_2O} = 0.65k_{obs} - 0.88$) introduced by Kimura et al.[36] With this equation, the calculated hydration number for **1** and **2** is ∼9.4 and for **3** and **4** is ∼7.9. Although speculative, it seems reasonable that the differences in the metal−water bond distances may account to some extent for these longer and shorter lifetimes. For example, because the prismatic waters are ∼3 pm closer to the yttrium ion in **2** than in **3**, and since we expect a corresponding shorter Cm−O(prism) distance in **2** than in **3** (cf. Table 1), this may cause a more efficient luminescence quenching process in the former host than in the latter.[39] We also note that the different hydrogen bonds between the water ligands and the anions in the second coordination shells may influence the lifetimes, as stronger hydrogen bonds weaken the intramolecular bonds of the water ligands and thus decrease their vibrational frequencies more than weaker hydrogen bonds, which may decrease the quenching efficiency of the waters and hence slightly increase the luminescence lifetime. An analogous effect (however in the opposite direction) was reported for Eu^{3+} and Cm^{3+} ions in aqueous perchloric solutions,[40] where the luminescence lifetimes were found to decrease with increasing concentration of perchlorate. Although the detailed mechanistic picture accounting for these effects is at present lacking, it is reasonable, however, to assume that this "anion effect", which gives rise to differences in the hydrogen bond strengths, does play a role for the luminescence decay rate in those perchloric-rich solutions as well as it does in the solids in the current study.

Comparisons with Cm^{3+}(aq). The fact that the peak shapes and the peak maxima of the emission spectra of **4** and the Cm^{3+} aqua ion are similar at room temperature suggests that the latter has a 9-fold, TTP coordination geometry. Indeed, the A_1-A_4 crystal-field levels of **4** and Cm^{3+}(aq) are similar (cf. Figures 2, 5, and 6 and ref 13). In addition, the band shapes of the excitation spectra of **2** and Cm^{3+}(aq) are comparable, again supporting a TTP geometry of the latter.[2] However, both its emission and excitation spectra are notably red-shifted relative to those of **1**−**3**, indicating that the polyhedral shape and the orientation of the capping waters are most likely not as those in **1**−**3**. In solution, the hydrogen bond structure between the first and second hydration spheres of Cm^{3+}(aq) is certainly different from those in **1**−**3**. Note that the orientation of the capping and prismatic waters and the ratio between the $M-O_c$/$M-O_p$ are very sensitive to the hydrogen bonding to the anions in the second coordination spheres in crystals. This is evident when comparing the $[Cm(H_2O)_9]^{3+}$ structures of **1**−**3** with that of **4** in Figure 1a.

However, the coordination geometry of Cm^{3+} in aqueous solution is relatively sensitive to temperature. It was recently shown that the peak maximum of the emission band of Cm^{3+}(aq) shifts from about 593.8 to 595.5 nm with increasing temperature from 20 to 200 °C; at 200 °C the peak maximum and the deduced positions of the A_1-A_4 levels were found to be similar to those of $[Cm(H_2O)_8]^{3+}$ in **5** at room temperature.[13] However,

for a more accurate comparison of how the local hydration structure of Cm^{3+} in aqueous solution at different temperatures and in solids influence their respective electronic level structures, it would be necessary to record extended UV−vis absorption spectra and/or excitation spectra to cover also the higher energy levels of Cm^{3+}. Carnall and Rajnak compared the UV−vis absorption spectra of Cm^{3+}(aq) and Cm^{3+} in $LaCl_3$ (in which the $[LaCl_9]^{6-}$ entity has C_{3h} symmetry) and found a pronounced resemblance,[41] suggesting a TTP coordination geometry for the Cm^{3+} aqua ion. We believe this qualitative comparison is justified. Reference compounds better suited to compare to the hydrated species in solution, $[Cm(H_2O)_9]^{3+}$ species with regular TTP coordination geometries are given in this work. A more complete discussion of the electronic levels of the Cm^{3+} spectra in these crystals given in this paper is in progress.

Summary and Conclusions

This paper presents the electronic level structures of the ground state ($S'_{7/2}$) and the first excited state ($^6D'_{7/2}$) multiplets of highly symmetric $[Cm(H_2O)_9]^{3+}$ species incorporated to the crystal lattices of the isotypic rare-earth salts $[La(H_2O)_9](CF_3SO_3)_3$ (**1**), $[Y(H_2O)_9](CF_3SO_3)_3$ (**2**), and $[Y(H_2O)_9](C_2H_5SO_4)_3$ (**3**), and species of low symmetry in $[La(H_2O)_9]Cl_3 \cdot 15\text{-crown-}5 \cdot H_2O$ (**4**). Comparisons are made to the recently published data of Cm^{3+}(aq)[2,13] and $[Cm(H_2O)_8]^{3+}$ in $[Y(H_2O)_8]Cl_3 \cdot 15\text{-crown-}5$ (**5**).[14] Detailed information about the crystal-field levels of the ground- and excited-state multiplets is obtained by $^6D'_{7/2} \rightarrow {}^8S'_{7/2}$ emission and $^8S'_{7/2} \rightarrow {}^6D'_{7/2}$ excitation spectra at 293 and 20 K. Excitation at low temperature is required in order to resolve the first (A_1) and second (A_2) crystal-field levels of the $^6D'_{7/2}$ multiplet; the A_3 and A_3 levels have very low absorptivity in these nonahydrates and their positions are not well defined at 20 K. The ground-state levels (Z_{1-4}) exhibit four sharp resonant lines at the A_1 and A_2 levels in the excitation spectra at 20 K. The total splittings of the ground and excited states are (in cm^{-1}) 8.0/376 (**1**), 6.0/391 (**2**), and 7.5/393 (**3**), which are significantly smaller than 35/656 for $[Cm(H_2O)_8]^{3+}$ in **5**.[14] We conclude that regular tricapped trigonal prismatic coordination geometries (D_{3h} and C_{3h} symmetries) with relatively large differences between the capping and prismatic metal−water distances cause weak crystal fields with small ground- and excited-state splittings. Hence, the total $^6D'_{7/2}$ splittings for **1**−**3** are smaller than those of the lower symmetry $[Cm(H_2O)_9]^{3+}$ ion in **4** (∼430 cm^{-1}) and Cm^{3+}(aq) (∼460 cm^{-1}),[13,2] consistent with weaker crystal fields in the former hosts than in **4** and in aqueous solution. These smaller splittings in **1**−**3** also explain the notable blue shifts of their emission spectra. These blue shifts, in turn, also show that the A_1 electronic level, the major emitting level in the fluorescence spectra, is very sensitive to small changes in the coordination geometry of $[Cm(H_2O)_9]^{3+}$ ions. In fact, the $^6D'_{7/2}$ splitting in the lanthanum host (**1**) is smaller than in the yttrium host (**2**), showing that the crystal-field strength around Cm^{3+} also depends on the size of the host metal ion: it increases as Cm^{3+} replaces a smaller host metal ion than itself, and vice versa. This size effect may be thought of as an "internal pressure" induced by the crystal lattice. Conversely, the splitting of the ground-state shows a reverse trend with a larger splitting in **1** than in **2**.

The luminescence lifetimes of $[Cm(H_2O)_9]^{3+}$ in **1** and **2** are similar to that of Cm^{3+}(aq), while the lifetimes are somewhat longer in **3** and **4**. Differences in the Cm−O distances and in the hydrogen bond strength between the water ligands and anions in the second coordination shells (anion effect) may account for the differences in the lifetimes.

Acknowledgment. We thank S. Büchner for technical assistance.

Supporting Information Available: Curve-fitted room temperature emission and excitation spectra of **1**−**4** (Figure S1) with fit parameters (Table S1), emission spectra of **2** recorded at different temperatures between 293 and 20 K (Figure S2), high-resolution emission spectrum of **3** at different delay times at 20 K (Figure S3), luminescence decay data of **1**−**4** (Figure S4), and crystallographic data of **4** in CIF format. This material is available free of charge via the Internet at http://pubs.acs.org.

References and Notes

(1) Skanthakumar, S.; Antonio, M. R.; Wilson, R. E.; Soderholm, L. *Inorg. Chem.* **2007**, *46*, 3485–3491.

(2) Lindqvist-Reis, P.; Apostolidis, C.; Rebizant, J.; Morgenstern, A.; Klenze, R.; Walter, O.; Fanghänel, T.; Haire, R. G. *Angew. Chem., Int. Ed.* **2007**, *46*, 919–922.

(3) Allen, P. G.; Bucher, J. J.; Shuh, D. K.; Edelstein, N. M.; Craig, I. *Inorg. Chem.* **2000**, *39*, 595–601.

(4) Antonio, M. R.; Soderholm, L.; Williams, C. W.; Blaudeau, J.-P.; Bursten, B. E. *Radiochim. Acta* **2001**, *89*, 17–25.

(5) Revel, R.; Auwer, C.; Den; Madic, C.; David, F.; Fourest, B.; Hubert, S.; Le Du, J.-F.; Morss, L. R. *Inorg. Chem.* **1999**, *38*, 4139–4141.

(6) Antonio, M. R.; Williams, C. W.; Soderholm, L. *Radiochim. Acta* **2002**, *90*, 851.

(7) Hagberg, D.; Bednarz, E.; Edelstein, N. M.; Gagliardi, L. *J. Am. Chem. Soc.* **2007**, *129*, 14136–14137.

(8) Yang, T.; Bursten, B. E. *Inorg. Chem.* **2006**, *45*, 5291–5301.

(9) Wiebke, J.; Mortiz, A.; Cao, X.; Dolg, M. *Phys. Chem. Chem. Phys.* **2007**, *9*, 459–465.

(10) Edelstein, N. M.; Klenze, R.; Fanghänel, T.; Hubert, S. *Coord. Chem. Rev.* **2006**, *250*, 948.

(11) (a) Sykora, R. E.; Assefa, Z.; Haire, R. G.; Albrecht-Schmitt, T. E. *J. Solid State Chem.* **2004**, *177*, 4413–4419. (b) Assefa, Z.; Haire, R. G.; Sykora, R. E. *J. Solid State Chem.* **2008**, *181*, 382–391.

(12) Like the Ln^{3+} aqua ions, the stability and kinetics of its first hydration sphere of the An^{3+} aqua ions is governed mainly by steric and electrostatic interactions. This gives rise to relatively high kinetic lability with considerably high exchange rates between the waters in the first and second hydration spheres; the TTP coordination geometry is thus the mean structure.

(13) Lindqvist-Reis, P.; Klenze, R.; Schubert, G.; Fanghänel, T. *J. Phys. Chem. B* **2005**, *109*, 3077–3083.

(14) Lindqvist-Reis, P.; Walther, C.; Klenze, R.; Eichhöfer, A.; Fanghänel, T. *J. Phys. Chem. B* **2006**, *110*, 5279–5285.

(15) Liu, G. K.; Beitz, J. V.; Huang, Jin *J. Chem. Phys.* **1993**, *99*, 3304–3311.

(16) Illemassene, M.; Murdock, K. M.; Edelstein, N. M.; Krupa, J. C. *J. Lumin.* **1997**, *75*, 77–87.

(17) Thouvenot, P.; Hubert, S.; Edelstein, N. M. *Phys. Rev. B* **1994**, *50*, 9715–9720.

(18) In an early EPR study of Cm^{3+} in $[La(H_2O)_9](C_2H_5SO_4)_3$, no details were given about the zero-field splitting of the $^8S'_{7/2}$ multiplet. Abraham, M.; Judd, B. R.; Wickman, H. H. *Phys. Rev.* **1963**, *130*, 611–612.

(19) (a) Harrowfield, J. M.; Kepert, D. L.; Patrick, J. M.; White, A. H. *Aust. J. Chem.* **1983**, *36*, 483. (b) Abbasi, A.; Lindqvist-Reis, P.; Eriksson, L.; Sandström, D.; Lidin, S.; Persson, I.; Sandström, M. *Chem. Eur. J.* **2005**, *11*, 4065–4077. (c) Persson, I.; D'Angelo, P.; Panfilis, S.; Sandström, M.; Eriksson, L. *Chem. Eur. J.* **2008**, *14*, 3056–3066.

(20) (a) Broach, R. W.; Williams, J. M. *Acta Crystallogr., Sect. B* **1979**, *35*, 2317–2321. (b) Gerkin, R. E.; Reppart, W. J. *Acta Crystallogr., Sect. C* **1984**, *40*, 781–786.

(21) Note that water deficiencies (x), triggered by the steric crowding between the water ligands, occur for Sc^{3+} and the smallest lanthanide ions, Lu^{3+}−Ho^{3+}, in the triflate series, $[M(H_2O)_{9-x}](CF_3SO_3)_3$ ($0 \le x \le 1$); see refs 19b and c.

(22) Matonic, J. H.; Scott, B. L.; Neu, M. P. *Inorg. Chem.* **2001**, *40*, 2638–2639.

(23) Rogers, R. D. *Inorg. Chim. Acta* **1988**, *149*, 307–314.

(24) The ^{248}Cm ($t_{1/2} = 3.40 \times 10^5$ years), which includes ∼9 wt % ^{246}Cm and some minor amounts of ^{243}Cm and ^{244}Cm isotopes, was obtained previously at FZK-INE by reprocessing of a used up ^{252}Cf neutron source.

(25) SMART, 5.046 (area detector control), SAINT, 5.01 (integration software), SADABS (empirical absorption correction program), SHELXTL, 5.1, Bruker Analytical X-ray Systems, Madison, WI, 1998.

(26) Crystal structure determination of **4**. $C_{10}H_{40}Cl_3LaO_{15}$, fw = 645.68 g mol^{-1}, orthorhombic, $a = 10.7084(14)$, $b = 15.3419(19)$, $c = 15.984(2)$ Å, $V = 2626.0(6)$ Å^3, $T = 295(2)$ K, space group $P2_12_12_1$ (No. 19), $Z = 4$,

ρ_{calc} = 1.628 g cm^{-1}, μ (Mo Kα) = 1.99 mm^{-1}, θ_{max} = 27.75°, 16483 reflections measured, 4393 reflections with $I > 2\sigma(I)$, 6035 independent reflections (R_{int} = 0.0386), 317 parameters, 45 restraints, $R[F^2 > 2\sigma(F^2)]$ = 0.034, w$R(F^2)$ = 0.077, S = 0.93.

(27) DIAMOND 2.1, Crystal Impact GbR, 2001.

(28) Abbasi, A.; Eriksson, L. *Acta Crystallogr., Sect. E* **2006**, *62*, i126–i128, and references therein.

(29) David, F. H.; Vokhmin, V. *New J. Chem.* **2003**, *27*, 1627–1632.

(30) Shannon, R. D. *Acta Crystallogr.* **1976**, *A32*, 751–767.

(31) An early luminescence and absorption spectroscopic paper on Cm^{3+} in $LaCl_3$ at 77 K reports all four crystal-filed levels (A_1-A_4) of the $^6D'_{7/2}$ multiplets at 16813, 16866, 16935, 16977 cm^{-1}; see: Gruber, J. B.; Cochran, W. R.; Conway, J. G.; Nicol, A. T. *J. Chem. Phys.* **1966**, *45*, 1423–1427.

(32) Binnemans, K.; Görller-Walrand, C. *Chem. Phys. Lett.* **1995**, *245*, 75–78.

(33) Auzel, F.; Malta, O. L. *J. Phys. (Paris)* **1983**, *44*, 201–206.

(34) This parameter may be used for comparisons of crystal-field strengths of different f^N ions in a given crystal host or for a particular f^N ion in different hosts, and it is proportional to the total (ΔE_{max}) splitting J levels with small J-mixing; N_v' is linearly related to N_v (defined in ref 33) according to $N_v' = N_v/(2\sqrt{\pi}) = (\sum_{k,q} (B^k_q)^2/(2k + 1))^{1/2}$.

(35) Hammond, R. M.; Reid, M. F.; Richardson, F. S. *J. Less-Common Met.* **1989**, *148*, 311.

(36) Kimura, T.; Choppin, G. R. *J. Alloys Compd.* **1994**, *213/214*, 313–317.

(37) Beitz, J. V. *Radiochim. Acta* **1991**, *52−53*, 35–39.

(38) An upper limit for k_r may be estimated, for example, in **2** where $k_{obs}(H_2O)$ = 15.6 ms^{-1} and $k_{obs}(D_2O)$ = 0.645 ms^{-1}, and since k_r is the same for the hydrated and deuterated compounds, k_r < 0.645 ms^{-1}. This value may be compared to that calculated for Cm^{3+}(aq), 0.769 ms^{-1}.

(39) Beeby, A.; Clarkson, I. M.; Dickins, R. S.; Faulkner, S.; Parker, D.; Royle, L.; de Sousa, A. S.; Williams, J. A. G.; Woods, M. *J. Chem. Soc., Perkin Trans. 2* **1999**, 493–503.

(40) (a) Giuliani, J. F.; Donohue, T. *Inorg. Chem.* **1978**, *17*, 1090–1091. (b) Breen, P. J.; Horrochs, W. D. *Inorg. Chem.* **1983**, *22*, 536–540. (c) Tanka, F.; Yamashita, S. *Inorg. Chem.* **1984**, *23*, 2044–2046. (d) Lis, S.; Choppin, G. R. *Mater. Chem. Phys.* **1992**, *31*, 159–161. (e) Nelig, A.; Elhabiri, M.; Billard, I.; Albrecht-Gary, A.-M.; Lützenkirchen, K. *Radiochim. Acta* **2003**, *91*, 37. (f) Kimura, T.; Kato, Y. *J. Alloys Compd.* **1998**, *278*, 92–97. (g) Kimura, T.; Kato, Y.; Takeishi, H.; Choppin, G. R. *J. Alloys Compd.* **1998**, *271−273*, 719–722. (h) For recent review, see: Billard, I. Lanthanide and Actinide Solution Chemistry Studied by Time-Resolved Emission Spectroscopy. In *Handbook on the Physics and Chemistry of Rare Earths*; Gschneidner, K. A., Jr., Bünzli, J.-C., Pecharsky, V. K., Eds.; Elsevier: Amsterdam, 2003; Vol. 33, Chapter 216, section 3.3.

(41) Carnall, W. T.; Rajnak, K. *J. Chem. Phys.* **1975**, *63*, 3510–3514.

JP808491K